Two-dimensional lattice Gross-Neveu model with domain-wall fermions

Taku Izubuchi*
Institute of Physics, University of Tsukuba, Tsukuba, Ibaraki 305-8571, Japan

Kei-ichi Nagai†
Institute of Physics, University of Tsukuba, Tsukuba, Ibaraki 305-8571, Japan
and Center for Computational Physics, University of Tsukuba, Tsukuba, Ibaraki 305-8577, Japan
(Received 18 June 1999; published 31 March 2000)

We investigate the two-dimensional lattice Gross-Neveu model in the large flavor number limit using the domain-wall fermion formulation as a toy model of lattice QCD. We study the nonperturbative behavior of the restoration of the chiral symmetry of the domain-wall fermions as the extent of the extra dimension (N_s) is increased to infinity. We find the parity broken phase (Aoki phase) for finite N_s, and study the phase diagram, which is related to the mechanism of chiral restoration in the $N_s \to \infty$ limit. The continuum limit is taken and the $O(a)$ scaling violation of observables vanishes in the $N_s \to \infty$ limit. We also examine the systematic dependencies of observables to the parameters.

PACS number(s): 11.15.Ha, 11.10.Kk, 11.15.Pg, 11.30.Rd

I. INTRODUCTION

Chiral symmetry is one of the important properties to understand hadron physics and the phase transition in the thermodynamics of field theories. Pions are regarded as pseudo Nambu-Goldstone bosons associated with the spontaneous breakdown of chiral symmetry. The physics of the phase transition between the confining phase (hadron phase) and the deconfining phase (quark-gluon plasma phase) in QCD is interesting from the theoretical and experimental points of view. Lattice field theory is one of the most powerful tools for such important physics beyond perturbations.

Defining chiral symmetry on the lattice, however, has been one of the long-standing problems in lattice field theory. This problem is known as the ''no-go theorem'' [1,2]: unwanted species of fermions appear in chiral symmetric theory on the lattice. To avoid this, chiral symmetry has to be broken by adding the Wilson term to the Lagrangian [3,4]. This formulation is known as the Wilson fermion (WF). In order to obtain the chiral symmetric theory in the continuum limit, one has to fine-tune the quark mass parameter to cancel the additive quantum correction, which is a nontrivial task in numerical simulations. Besides this fine-tuning difficulty, the physical prediction from the WF has $O(a)$ scaling violation due to the absence of chiral symmetry, where a is the lattice spacing. One must calculate on a fine lattice to get precise predictions in the WF.

Several years ago, the domain-wall fermion (DWF) was proposed [5,6] as a new formulation of the lattice fermion. The DWF is formulated as a $(D+1)$-dimensional Wilson fermion with the free boundary condition in the extra dimension [6]. In this model each of two chiral modes is expected to localize at each boundary of extra dimension separately, and if the localization is exponential, chiral symmetry (massless fermion) on the lattice is realized in the $N_s \to \infty$ limit. This expectation is easily checked in the free fermion case. The stability of the chiral symmetry under perturbative gauge fluctuations is checked manifestly in the DWF case [7] and in the overlap formula [8–11]. This radiative stability is a result of an internal supersymmetry [12] in the infinite extra direction when the DWF is just an overlap fermion. Because of these properties, the current quark mass term in the DWF receives multiplicative renormalization in contrast with the WF, and this fermion formulation does not need a fine-tuning in order to restore chiral symmetry on the lattice [7,13]. The $O(a)$ scaling violation is expected to vanish in the large N_s limit, which means smaller scaling violations than in the WF. Thus the DWF has the desirable property for defining the lattice fermion especially for chiral symmetric or near massless cases.

Numerical simulations of the domain-wall QCD (DWQCD) have been already carried out [14,15]. As a trade-off of the above ideal properties, one needs a large amount of CPU time for computer simulations of DWQCD. Furthermore, the new model has a larger number of parameters than that of the WF, and the results of simulations have complicated dependences on parameters.

To clarify the nonperturbative properties of DWQCD, we examine the formalism for the solvable theory, Gross-Neveu (GN) model in two dimensions, which shares a common nature with QCD. Our main purpose in this paper is to understand the restoration of chiral symmetry. For finite N_s, for which the lattice simulations are performed, we will see that chiral symmetry is broken, and the model can be seen as an ''improved Wilson fermion.'' (The finite N_s effects in the truncated overlap formalism are mentioned in Ref. [11].) DWF for finite N_s has a parity broken phase similar to the WF [16–18]. We also study the continuum limit of the DWF model. We will see the $O(a)$ scaling violation becomes small as N_s is increased and vanishes in the limit $N_s \to \infty$.

This paper is organized as follows: In Sec. II, after a brief review of the GN model in the continuum, the lattice GN

*Email address: izubuchi@het.ph.tsukuba.ac.jp
†Email address: nagai@rccp.tsukuba.ac.jp

model with the DWF is formulated and the effective potentials in the large flavor (N) limit are calculated when the extent of extra dimensions (N_s) is both infinite and finite. In Sec. III we calculate the continuum limit in the infinite and finite N_s cases and discuss the restoration of chiral symmetry. We will see that the model has chiral symmetry on the lattice for infinite N_s, while the symmetry is restored only in the continuum limit with fine-tuning for finite N_s. In Sec. IV we analyze the structure of the chiral phase boundary between the parity symmetric and the parity broken phase (Aoki phase) for finite lattice spacing by solving the gap equation and discuss the necessity of fine-tuning to restore the chiral symmetry. In Sec. V we study the parameter dependences of the lattice observables and in Sec. VI we discuss the way of taking the continuum limit. We will see that the correct continuum limit is taken from the lattice model and the $O(a)$ scaling violation vanishes for the $N_s \to \infty$ limit. We conclude with a summary in Sec. VII.

II. ACTION AND THE EFFECTIVE POTENTIAL

A. Continuum Gross-Neveu model

Investigation of the GN model is a good test [16,19–22] for the nonperturbative behavior of QCD since the two theories share common properties: the feature of asymptotic freedom, chiral symmetry, and its spontaneous breakdown.

The two-dimensional continuum Gross-Neveu model in Euclidean space is defined by the action

$$S=\int dx^2\left\{\bar{\psi}(\gamma_\mu\partial_\mu+m)\psi-\frac{g^2}{2N}[(\bar{\psi}\psi)^2+(\bar{\psi}i\gamma_5\psi)^2]\right\}, \tag{1}$$

where ψ is an N-component fermion field. The effective potential in the large N limit in the continuum theory is given as

$$V_{eff}=-m\sigma+\frac{1}{4\pi}(\sigma^2+\Pi^2)\ln\frac{\sigma^2+\Pi^2}{e\Lambda^2}, \tag{2}$$

where m is the renormalized mass and Λ is the scale parameter. If the momentum integration is regularized by a cutoff M, the renormalization for bare mass m_0 and the bare coupling constant g^2 are

$$m=\frac{m_0}{g^2}, \tag{3}$$

$$\frac{1}{g^2}=\frac{1}{2\pi}\ln\frac{M^2}{\Lambda^2}, \tag{4}$$

where the latter is asymptotically free. (We set the renormalized coupling constant to unity.)

The auxiliary fields σ and Π relate to the fermion condensations by the equation of motion

$$\sigma=m_0-\frac{g^2}{N}\bar{\psi}\psi, \quad \Pi=-\frac{g^2}{N}\bar{\psi}i\gamma_5\psi. \tag{5}$$

When m_0 vanishes the model shows chiral symmetry, which is expressed by the $O(2)$ rotational invariance of the effective action (2) in (σ,Π) space. The stationary point of the effective action (2) satisfies $\sigma^2+\Pi^2=\Lambda^2$, which manifests the spontaneous breakdown of chiral symmetry.

B. Lattice model with the DWF

The DWF is formulated as a Wilson fermion in $D+1$ dimensions or, equivalently, N_s flavor WF with a flavor mixing, which has a negative Wilson term obeying the free boundary condition on the edges in the extra dimension [6].

The action of the DWF is given as follows:

$$S_{\text{free}}=a^2\sum_{s,t}\sum_{m,n}\bar{\psi}(m,s)D^{free}(m,s;n,t)\psi(n,t), \tag{6}$$

where

$$D^{free}(m,s;n,t)=\sum_{\mu=1}^{2}\sigma_\mu C_\mu(m,n)\delta_{s,t}-W(m,n)\delta_{s,t}+P_R\delta_{s+1,t}\delta_{m,n}+P_L\delta_{s,t+1}\delta_{m,n}, \tag{7}$$

$$C_\mu(m,n)=\frac{a_s}{2a}[\delta_{m+\hat{\mu},n}-\delta_{m-\hat{\mu},n}], \tag{8}$$

$$W(m,n)=(1-M)\delta_{m,n}+\frac{ra_s}{2a}[2\delta_{m,n}-\delta_{m+\hat{\mu},n}-\delta_{m,n+\hat{\mu}}]. \tag{9}$$

$P_{R/L}=(1\pm\gamma_5)/2$ are the projection operators into the right- and the left-handed modes, and a and a_s are the lattice spacing in two and three dimensions, respectively. σ_μ's are defined as $\sigma_1=i$ and $\sigma_2=1$ in two dimensions; s and t are the indicies of extra dimension with $1\leqslant s,t\leqslant N_s$. Here, $r(>0)$ is Wilson coupling constant and M is the domain-wall mass height (DW mass). The boundary condition in the third direction takes the free boundary condition. In the following, we take $a=a_s$ and $r=1$ for simplicity.

If one sets $0<M<2$, there is *single* light Dirac fermion in the spectrum of this free action whose right- (left-) handed component stays near $s=1(N_s)$,

$$q(n)=P_R\psi(n,s=1)+P_L\psi(n,s=N_s). \tag{10}$$

The mass of this light quark, $q(n)$, is exponentially suppressed for large N_s,

$$m_q a\sim(1-M)^{N_s}. \tag{11}$$

The Wilson term in the action avoids the species doubling problem. The doublers and other N_s-1 bulk fermions acquire the cutoff order mass and decouple from low energy physics.

As a toy model of the lattice DWQCD, we define the two-dimensional lattice GN model with N flavors:

$$S=S_{free}+a^2\sum_n m_f\bar{q}(n)q(n)-a^2\sum_n\left[\frac{g_\sigma^2}{2N}\{\bar{q}(n)q(n)\}^2+\frac{g_\pi^2}{2N}\{\bar{q}(n)i\gamma_5 q(n)\}^2\right], \tag{12}$$

where we abbreviate $\bar{\psi}(n,s)\psi(n,t)=\Sigma_{i=1}^N\bar{\psi}^i(n,s)\psi^i(n,t)$. m_f is the ''current quark mass'' in order to give mass to the fermion.[1] In the perturbation of DWQCD, m_f receives the multiplicative renormalization in the $N_s\to\infty$ case [7,13]. The DW mass M, on the other hand, receives the additive renormalization [7,13], because M corresponds to the Wilson mass term. We will see that two different couplings g_σ^2 and g_π^2 are needed for chiral symmetry in general.

The action (12) can be rewritten in the following equivalent action using the auxiliary fields $\sigma(n)$ and $\Pi(n)$:

$$S=S_{\rm free}+a^2\sum_n\bar{q}(n)\{a\sigma(n)+i\gamma_5 a\Pi(n)\}q(n)+a^2\sum_n\left[\frac{N}{2g_\sigma^2}\{\sigma(n)-m_f\}^2+\frac{N}{2g_\pi^2}\Pi(n)^2\right]. \tag{13}$$

The auxiliary fields are related to condensation of fermions,

$$\sigma(n)=m_f-\frac{g_\sigma^2}{N}\bar{q}(n)q(n),\quad \Pi(n)=-\frac{g_\pi^2}{N}\bar{q}(n)i\gamma_5 q(n), \tag{14}$$

from the equations of motion.

C. Effective potential

We calculate the effective potential of the two-dimensional lattice GN model in the large N limit. In the large N limit, in which the quantum fluctuation of $\sigma(n)$ and $\Pi(n)$ is suppressed and the mean field approximation $\sigma(n)\to\sigma$ and $\Pi(n)\to\Pi$ becomes exact, the effective potential of the GN model is obtained by exponentiating the fermion determinant which is calculated by integration of the fermion fields ψ:

$$\begin{aligned}Z&=\int[d\psi][d\bar{\psi}]\exp\left(-a^2\sum\bar{\psi}D\psi\right)\\&\quad\times\exp\left(-a^2\sum\left[\frac{N}{2g_\sigma^2}(\sigma-m_f)^2+\frac{N}{2g_\pi^2}\Pi^2\right]\right)\\&=\det D(\sigma,\Pi)\\&\quad\times\exp\left(-a^2\sum\left[\frac{N}{2g_\sigma^2}(\sigma-m_f)^2+\frac{N}{2g_\pi^2}\Pi^2\right]\right)\\&=e^{-a^2V_{eff}}.\end{aligned} \tag{15}$$

[1]The parameters M, r, and m_f in this paper are opposite in sign from those of Ref. [23].

This determinant can be calculated by employing the technique of the propagator matrix [11,24]. The action introduced in the previous subsection is rewritten by the matrix representation, in the momentum space. From Eq. (13),

$$\begin{aligned}S&=\bar{\psi}D(\sigma,\Pi)\psi\\&=a^2\sum_{s,t}\sum_p(\psi_L^\dagger(-p,s),\psi_R^\dagger(-p,s))\left[\begin{pmatrix}C^\dagger&-W\\-W&-C\end{pmatrix}\delta_{s,t}\right.\\&\quad+\begin{pmatrix}0&0\\1&0\end{pmatrix}\delta_{s+1,t}+\begin{pmatrix}0&1\\0&0\end{pmatrix}\delta_{s-1,t}+\begin{pmatrix}0&0\\a\omega&0\end{pmatrix}\delta_{s,N}\delta_{t,1}\\&\quad\left.+\begin{pmatrix}0&a\omega^\dagger\\0&0\end{pmatrix}\delta_{s,1}\delta_{t,N_s}\right]\begin{pmatrix}\psi_R(p,t)\\\psi_L(p,t)\end{pmatrix},\end{aligned} \tag{16}$$

where $C^\dagger=\sin(p_1a)+i\sin(p_2a)$, $\omega=\sigma+i\Pi$, and $W=(1-M)+\Sigma_{\mu=1}^2[1-\cos(p_\mu a)]$. Similarly to Refs. [11,24], we can calculate the effective action of this model. The kernel of the action D can be written in the following matrix form:

$$\sigma_1 D=\begin{pmatrix}C^\dagger&-W&0&\cdots&\cdots&0&a\omega^\dagger\\-W&-C&1&0&\cdots&0&0\\0&1&C^\dagger&-W&0&\cdots&0\\\cdots&0&-W&-C&1&\cdots&0\\\cdots&\cdots&\cdots&\ddots&\ddots&\cdots&\cdots\\0&\cdots&\cdots&0&1&C^\dagger&-W\\a\omega&0&\cdots&\cdots&0&-W&-C\end{pmatrix}. \tag{17}$$

The fermionic determinant is obtained by moving the first column in matrix (17) to the last,

$$\det(\sigma_1 D)=(-1)^{q(N_s-1)}\times\det\begin{pmatrix}\alpha&0&\cdots&\cdots&0&\beta'\\\beta&\alpha&0&\cdots&\cdots&0\\0&\beta&\alpha&0&\cdots&0\\\cdots&\ddots&\ddots&\ddots&\cdots&\cdots\\\cdots&\cdots&0&\beta&\alpha&0\\0&\cdots&\cdots&0&\beta&\alpha'\end{pmatrix}, \tag{18}$$

where $q=N_cL^D$ $(N_c=1,D=2)$ and

$$\alpha=\begin{pmatrix}-W&0\\-C&1\end{pmatrix},\quad \alpha'=\begin{pmatrix}-W&0\\-C&a\omega\end{pmatrix}, \tag{19}$$

$$\beta=\begin{pmatrix}1&C^\dagger\\0&-W\end{pmatrix},\quad \beta'=\begin{pmatrix}a\omega^\dagger&C^\dagger\\0&-W\end{pmatrix}. \tag{20}$$

If we decompose the matrix (18) into two matrices,

$$\begin{pmatrix} \alpha & 0 & \cdots & \cdots & 0 & \beta' \\ \beta & \alpha & 0 & \cdots & \cdots & 0 \\ 0 & \beta & \alpha & 0 & \cdots & 0 \\ \cdots & \ddots & \ddots & \ddots & \cdots & \cdots \\ \cdots & \cdots & 0 & \beta & \alpha & 0 \\ 0 & \cdots & \cdots & 0 & \beta & \alpha' \end{pmatrix}$$

$$= \begin{pmatrix} \alpha & 0 & \cdots & \cdots & 0 & 0 \\ \beta & \alpha & 0 & \cdots & \cdots & 0 \\ 0 & \beta & \alpha & 0 & \cdots & 0 \\ \cdots & \ddots & \ddots & \ddots & \cdots & \cdots \\ \cdots & \cdots & 0 & \beta & \alpha & 0 \\ 0 & \cdots & \cdots & 0 & \beta & \alpha' \end{pmatrix} \times \begin{pmatrix} 1 & 0 & \cdots & \cdots & 0 & -v_1 \\ 0 & 1 & 0 & \cdots & 0 & -v_2 \\ \cdots & 0 & 1 & 0 & \cdots & -v_3 \\ \cdots & \ddots & \ddots & \ddots & \cdots & \cdots \\ \cdots & \cdots & \cdots & 0 & 1 & -v_{N_s-1} \\ 0 & \cdots & \cdots & \cdots & 0 & 1-v_{N_s} \end{pmatrix}, \tag{21}$$

where

$$v_1 = -\alpha^{-1}\beta', \tag{22}$$

$$v_i{}^{-1}\beta v_{i-1} \quad (2 \leqslant i \leqslant N_s - 1), \tag{23}$$

$$v_{N_s} = -\alpha'^{-1}\beta v_{N_s-1} = (-\alpha'^{-1}\beta)(-\alpha^{-1}\beta)^{N_s-2}(-\alpha^{-1}\beta'), \tag{24}$$

we obtain the determinant as follows:

$$\det(\sigma_1 D) = (-1)^{q(N_s-1)}(\det\alpha)^{N_s-1}\det\alpha'\det(1-v_{N_s}). \tag{25}$$

The final expression of the fermionic determinant is

$$\det D(\sigma,\Pi) = \det\left[\begin{pmatrix} a\omega & 0 \\ 0 & 1 \end{pmatrix} - T^{-N_s}\begin{pmatrix} 1 & 0 \\ 0 & a\omega^\dagger \end{pmatrix}\right], \tag{26}$$

where T is the transfer matrix along the extra dimension defined by

$$T = e^{a_s H_s} = \begin{pmatrix} \frac{1}{W}, & -\frac{1}{W}C \\ -C^\dagger\frac{1}{W}, & W + C^\dagger\frac{1}{W}C \end{pmatrix},$$

$$T^{-1} = \begin{pmatrix} C^\dagger\frac{1}{W}C + W, & C\frac{1}{W} \\ \frac{1}{W}C^\dagger, & \frac{1}{W} \end{pmatrix}. \tag{27}$$

We omit overall factors independent of the fields σ and Π in Eq. (26). H_s is the Hamiltonian which generates the transfer along the extra dimension. Diagonalizing T^{-1}, whose eigenvalues are λ and $1/\lambda$, we obtain an explicit formula for the determinant,

$$\det D(\sigma,\Pi) = \prod_{p_\mu}[F(M,N_s,p_\mu)a^2(\sigma^2+\Pi^2) + G(M,N_s,p_\mu)a\sigma + H(M,N_s,p_\mu)], \tag{28}$$

where

$$H(M,N_s,p_\mu) = \frac{-1}{2f}[-(\lambda^{N_s}-\lambda^{-N_s})(2-h) + (\lambda^{N_s}+\lambda^{-N_s})f], \tag{29}$$

$$F(M,N_s,p_\mu) = \frac{-1}{2f}[(\lambda^{N_s}-\lambda^{-N_s})(2-h) + (\lambda^{N_s}+\lambda^{-N_s})f], \tag{30}$$

$$G(M,N_s,p_\mu) = \frac{-1}{2f}[-4f] = 2, \tag{31}$$

$$h = 1 + W^2 + \overline{p^2}, \quad f = \sqrt{-4W^2 + h^2}, \tag{32}$$

$$\lambda = \frac{1}{2W}[h+f] \quad (|\lambda| > 1),$$

$$\frac{1}{\lambda} = \frac{1}{2W}[h-f], \tag{33}$$

$$W = (1-M) + \sum_{\mu=1}^{2}[1-\cos(p_\mu a)],$$

$$\overline{p^2} = \sin^2(p_1 a) + \sin^2(p_2 a). \tag{34}$$

Substituting Eq. (28) into Eq. (15), we obtain the effective potential of the two-dimensional lattice GN model in the large N limit:

$$V_{eff} = \frac{1}{2g_\sigma^2}(\sigma - m_f)^2 + \frac{1}{2g_\pi^2}\Pi^2 - I(\sigma,\Pi,M,N_s), \tag{35}$$

$$I(\sigma,\Pi,M,N_s) = \int_{-\pi/a}^{\pi/a}\frac{d^2p}{(2\pi)^2} \times \ln[Fa^2(\sigma^2+\Pi^2) + Ga\sigma + H]. \tag{36}$$

This effective potential is symmetric under $M \to 6 - M$.

Here we comment about the absence of the bosonic fields (Pauli-Villars fields) in our model which is employed in (full) QCD [13–15]. Since the gauge field in QCD equally interacts with not only the light quark field $q(n)$, but also heavy (bulk) fermions $\psi(n,s)$, one should introduce the Pauli-Villars boson to subtract this heavy fermion effect. In

the GN model σ and Π play an analogous role to the gauge field in full QCD except that they couple with $q(n)$ only. Thus it is not necessary to introduce subtraction in our model. On the other hand, one could think about a new four Fermi interaction model, in which whole $\psi(n,s)$, $s=1,\ldots,N_s$, equally couple to auxiliary fields σ and Π. However, these fields are constituted of both light and heavy fermions and do not show the chiral property in such a new model.

III. CHIRAL SYMMETRY RESTORATION

First we show how chiral symmetry is restored in this model in the case of *both* $N_s=\infty$ and $N_s<\infty$ by examining the effective potential given in the previous section.

We will see that for the infinite N_s case chiral symmetry is exact even for finite lattice spacing, $a>0$, without fine-tuning for bare mass parameters. The situation for the finite N_s case, on the other hand, is much like that of the Wilson fermion action. The continuum limit has to be taken, and at the same time, the bare mass parameter must be tuned finely for the chiral symmetric effective potential for $N_s<\infty$.

A. Effective potential in the "$N_s=\infty$" case

In this subsection we calculate the expression of the effective potential for the $N_s=\infty$ case.

For large N_s, one easily sees that the dominant contributions for the function $I(\sigma,\Pi)$ in the effective potential (36) are the functions "F" and "H," which behave as λ^{N_s} in the $N_s\to\infty$ limit, from Eqs. (29) and (30). The chiral breaking term "$Ga\sigma$" in Eq. (36) can be ignored in the limit $N_s\to\infty$ and Eq. (36) could be written as

$$I(\sigma,\Pi)=\int_{-\pi/a}^{\pi/a}\frac{d^2p}{(2\pi)^2}\ln[H+Fa^2(\sigma^2+\Pi^2)]. \quad (37)$$

So the effective potential (35) is a function of $\sigma^2+\Pi^2$, which is invariant under the $O(2)$ rotation if $g_\sigma^2=g_\pi^2$. We emphasize that this is chiral symmetry even before taking the continuum limit, $a\to 0$.

The continuum limit of the effective potential can be evaluated by separating divergent parts and finite parts from Eq. (37). Rewriting Eq. (37) in an integration form

$$I(\sigma,\Pi)=\int_0^{\sigma^2+\Pi^2}d\rho\ K(\rho),\quad K(\rho)$$
$$=\int_{-\pi/a}^{\pi/a}\frac{d^2p}{(2\pi)^2}\frac{1}{\dfrac{H}{Fa^2}+\rho}, \quad (38)$$

one can pick up the the divergent part in the $a\to 0$, near zero fermion momentum, $p_\mu a=(0,0)$, for $\rho a^2\sim 0$. Since the divergent part of $K(\rho)$ behaves as

$$\frac{H}{Fa^2}\to\frac{1}{M^2(2-M)^2}\sum_{\mu=1}^{2}p_\mu^2, \quad (39)$$

in the $a\to 0$ limit, the function $K(\rho)$ becomes

$$K(\rho)=\int_{-\pi/a}^{\pi/a}\frac{d^2p}{(2\pi)^2}\frac{1}{f_M^{-2}\sum_{\mu=1}^{2}p_\mu^2+\rho}+C_0(M,N_s), \quad (40)$$

where $f_M=M(2-M)$ and

$$C_0(M,N_s)=\int_{-\pi}^{\pi}\frac{d^2\xi}{(2\pi)^2}\frac{f_M^{-2}\sum_\mu\xi_\mu^2-\dfrac{H}{F}}{\dfrac{H}{F}f_M^{-2}\sum_\mu\xi_\mu^2}, \quad (41)$$

with $\xi_\mu=p_\mu a$. The factor f_M appears as the normalization factor of the propagator: $\langle q\bar{q}\rangle\sim f_M(ip_\mu\gamma_\mu)^{-1}$. The wave function of the massless eigenmode has finite width in the s direction, and f_M is the ratio of $q(n)$ to the zero mode.

In the $N_s=\infty$ case, when $0<M<2$, only the momentum around $p_\mu a=(0,0)$ dominates in eq. (37) and the contributions of doublers, $p_\mu a=(\pi,0)$, $(0,\pi)$, and (π,π), are removed completely. This means that the doublers decouple from the physical spectrum. For $2<M<4$ the momenta $p_\mu a=(\pi,0)$ and $(0,\pi)$ become physical poles in the momentum integral, while the remaining mode at $p_\mu a=(\pi,\pi)$ is dominant for $4<M<6$. In these two regions of M, the normalization factor f_M becomes $(M-2)(4-M)$ and $(M-4)(6-M)$, respectively. For $M<0$ and $M>6$, no physical pole emerges.

By evaluation of the first term on the right hand side (RHS) in Eq. (40), we find

$$K(\rho)=\frac{f_M^2}{4\pi}\ln\frac{1}{a^2f_M^2\rho}+\hat{C}_0(M,N_s), \quad (42)$$

where the new constant $\hat{C}_0$ is defined by $\hat{C}_0=C_0+C_0'$ with

$$\int_{-\pi/a}^{\pi/a}\frac{d^2p}{(2\pi)^2}\frac{1}{f_M^{-2}\sum_{\mu=1}^{2}p_\mu^2+\rho}\equiv\frac{f_M^2}{4\pi}\ln\frac{1}{a^2f_M^2\rho}+C_0'(M,N_s). \quad (43)$$

By substituting this expression into Eq. (38), we obtain

$$I=-\frac{f_M^2}{4\pi}(\sigma^2+\Pi^2)\ln\frac{a^2f_M^2(\sigma^2+\Pi^2)}{e}+\hat{C}_0(\sigma^2+\Pi^2). \quad (44)$$

Therefore the continuum limit of the effective potential for the $N_s=\infty$ case is

$$V_{eff}=-\frac{m_f}{g^2}\sigma+\left(\frac{1}{2g^2}-\hat{C}_0+\frac{f_M^2}{4\pi}\ln a^2\right)(\sigma^2+\Pi^2)$$
$$+\frac{f_M^2}{4\pi}(\sigma^2+\Pi^2)\ln\frac{f_M^2(\sigma^2+\Pi^2)}{e}. \quad (45)$$

We find that the two coupling constants can be the same as each other, $g^2=g_\sigma^2=g_\pi^2$, from the above result, which is in contrast to the GN model with the WF. As mentioned above, since the effective potential has chiral symmetry for finite lattice spacing, fine-tuning is unnecessary for the chiral symmetric continuum limit.

After redefining for σ and Π such as $\sigma_R=f_M\sigma$ and $\Pi_R=f_M\Pi$, we renormalize the coupling constant g and m_f as follows:

$$\frac{1}{2g^2}=\hat{C}_0+\frac{f_M^2}{4\pi}\ln\frac{1}{a^2\Lambda^2}, \tag{46}$$

$$m=\frac{m_f}{f_M g^2}=m_f\left(\frac{2}{f_M}\hat{C}_0+\frac{f_M}{2\pi}\ln\frac{1}{a^2\Lambda^2}\right), \tag{47}$$

where Λ is the scale parameter and m is the renormalized mass parameter. One realizes that the current quark mass term m_f receives a multiplicative renormalization (47), similar to perturbation theory in infinitely large N_s. With this choice of scaling relations the continuum limit of the effective potential for $N_s=\infty$ is finally given as

$$V_{eff}=-m\sigma_R+\frac{1}{4\pi}(\sigma_R^2+\Pi_R^2)\ln\frac{\sigma_R^2+\Pi_R^2}{e\Lambda^2}, \tag{48}$$

which is identical to the continuum theory (2).

B. Chiral restoration in the continuum limit (N_s finite case)

As we have seen in the previous subsection, the limit $N_s\to\infty$ guarantees chiral symmetry on a lattice. Nevertheless, to understand the behavior of finite N_s theory is important for lattice QCD simulations using DWF.

Let us start the finite N_s analysis with the effective potential (35). The chiral breaking term $Ga\sigma$ in Eq. (36) has an important role for finite N_s and the GN model does not have chiral symmetry anymore. Chiral symmetry can be restored in the continuum limit with fine-tuning. In this sense, the finite N_s model is similar to the WF. In order to restore chiral symmetry without fine-tuning, one should take the limit $N_s\to\infty$ *before* taking the continuum limit to obtain chiral symmetry on the lattice.

The continuum limit for finite N_s can be taken following the same procedures in the previous subsection. The difference from the calculation in $N_s\to\infty$ is a necessity to shift the auxiliary field:

$$\sigma'=\sigma-\frac{(1-M)^{N_s}}{a}. \tag{49}$$

The effective potential becomes as follows:

$$V_{eff}=\frac{1}{2g_\sigma^2}\left\{\sigma'-\left(m_f-\frac{(1-M)^{N_s}}{a}\right)\right\}^2+\frac{1}{2g_\pi^2}\Pi^2-I(\sigma,\Pi), \tag{50}$$

$$I(\sigma,\Pi)=\int_{-\pi/a}^{\pi/a}\frac{d^2p}{(2\pi)^2}\ln[H'+Fa^2(\sigma'^2+\Pi^2)+G'a\sigma'], \tag{51}$$

where

$$H'=H+F(1-M)^{2N_s}+G(1-M)^{N_s},$$
$$G'=G+2F(1-M)^{N_s}. \tag{52}$$

Expanding $I(\sigma,\Pi)$ into a power series of lattice spacing,

$$I=I_0+I_1+I_2+\cdots, \tag{53}$$

$$I_0=\int_{-\pi/a}^{\pi/a}\frac{d^2p}{(2\pi)^2}\ln[H'+Fa^2(\sigma'^2+\Pi^2)], \tag{54}$$

$$I_n=-\frac{(-1)^n}{n}\int_{-\pi/a}^{\pi/a}\frac{d^2p}{(2\pi)^2}\left[\frac{G'a\sigma'}{H'+Fa^2(\sigma'^2+\Pi^2)}\right]^n \quad (n\geqslant 1). \tag{55}$$

One can see that I_0 preserve the $O(2)$ rotation in the (σ',Π) plane, while I_n $(n\geqslant 1)$ break it.

I_0 is calculated in the same way as in the $N_s=\infty$ case:

$$I_0=\int_0^{\sigma'^2+\Pi^2}d\rho\ K(\rho),\quad K(\rho)=\int_{-\pi/a}^{\pi/a}\frac{d^2p}{(2\pi)^2}\frac{1}{\frac{H'}{Fa^2}+\rho}. \tag{56}$$

Here we take the divergent part in $a\to 0$. The shifted function H' has a similar behavior to the limit $N_s\to\infty$:

$$\frac{H'}{Fa^2}\to f_M^{-2}\sum_\mu p_\mu^2, \tag{57}$$

with

$$f_M=\frac{M(2-M)}{1-(1-M)^{2N_s}}. \tag{58}$$

Therefore the logarithmic divergent term has a similar form as continuum theory:

$$I_0=-\frac{f_M^2}{4\pi}(\sigma'^2+\Pi^2)\ln\frac{a^2f_M^2(\sigma'^2+\Pi^2)}{e}+\hat{C}_0(\sigma'^2+\Pi^2), \tag{59}$$

where the new constant $\hat{C}_0$ is defined by $\hat{C}_0=C_0+C_0'$ with

$$C_0(M,N_s)=\int_{-\pi}^{\pi}\frac{d^2\xi}{(2\pi)^2}\frac{f_M^{-2}\sum_\mu\xi_\mu^2-\frac{H'}{F}}{\frac{H'}{F}f_M^{-2}\sum_\mu\xi_\mu^2} \tag{60}$$

and

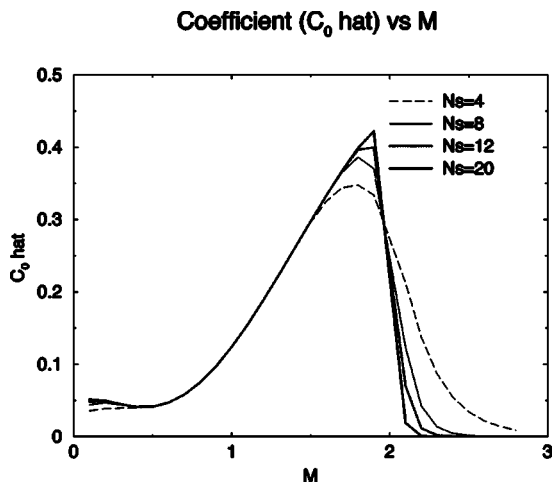

FIG. 1. The coefficient, $\hat{C}_0$, as a function of M for various N_s.

$$\int_{-\pi/a}^{\pi/a}\frac{d^2p}{(2\pi)^2}\frac{1}{f_M^{-2}\sum_{\mu=1}^{2}p_\mu^2+\rho}\equiv\frac{f_M^2}{4\pi}\ln\frac{1}{a^2f_M^2\rho}+C_0'(M,N_s). \tag{61}$$

The coefficient $\hat{C}_0$ as a function of M for various N_s is plotted in Fig. 1.

I_n remaining in the continuum limit is easily calculated. I_1 (I_2) is a linear divergent (constant) term in the $a\to 0$ limit, while I_n ($n\geqslant 3$) vanishes:

$$I_1=\frac{\sigma'}{a}C_1=\frac{\sigma'}{a}\int_{-\pi}^{\pi}\frac{d^2\xi}{(2\pi)^2}\frac{G'}{H'}, \tag{62}$$

$$I_2=-\sigma'^2C_2=-\sigma'^2\frac{1}{2}\int_{-\pi}^{\pi}\frac{d^2\xi}{(2\pi)^2}\left[\frac{G'}{H'}\right]^2. \tag{63}$$

Figure 2 shows these coefficients as a function of N_s for various M.

From the above calculations, the effective potential in the finite N_s case in the continuum limit is obtained as follows:

$$\begin{aligned}V_{eff}=&-\left(\frac{m_f'}{g_\sigma^2}+\frac{C_1}{a}\right)\frac{1}{f_M}\sigma_R+\left(\frac{1}{2g_\sigma^2}-\hat{C}_0+C_2\right)\frac{1}{f_M^2}\sigma_R^2\\&+\left(\frac{1}{2g_\pi^2}-\hat{C}_0\right)\frac{1}{f_M^2}\Pi_R^2+\frac{1}{4\pi}(\sigma_R^2+\Pi_R^2)\\&\times\ln\frac{a^2(\sigma_R^2+\Pi_R^2)}{e},\end{aligned} \tag{64}$$

where

$$m_f'=m_f-\frac{(1-M)^{N_s}}{a},\quad \sigma_R=f_M\sigma',\quad \Pi_R=f_M\Pi. \tag{65}$$

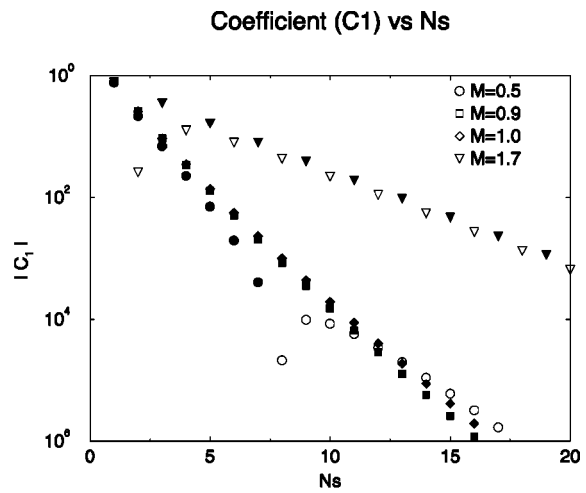

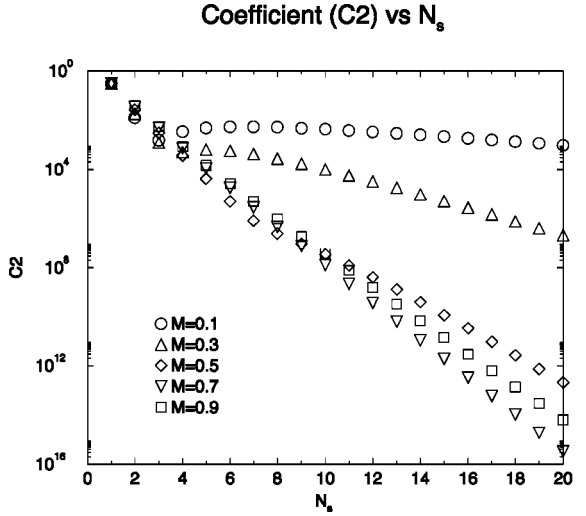

FIG. 2. The coefficients, C_1 and C_2, as a function of N_s for fixed values of M. The data for C_1 are plotted as absolute values and solid symbols denote $C_1<0$.

If the coupling constants and the mass parameter are renormalized as

$$\frac{1}{2g_\sigma^2}-\hat{C}_0+C_2=\frac{f_M^2}{4\pi}\ln\frac{1}{a^2\Lambda^2}, \tag{66}$$

$$\frac{1}{2g_\pi^2}-\hat{C}_0=\frac{f_M^2}{4\pi}\ln\frac{1}{a^2\Lambda^2}, \tag{67}$$

$$\frac{1}{f_M}\left(\frac{m_f'}{g_\sigma^2}+\frac{C_1}{a}\right)=m, \tag{68}$$

we obtain the correct effective potential of the continuum theory (2).

We emphasize that the current quark mass term m_f receives $O(1/a)$ additive renormalization for the $N_s=$finite case. As we described previously, fine-tuning for the bare mass parameter in Eq. (68) is needed for finite N_s, and chiral symmetry is restored in the continuum limit.

The restoration of chiral symmetry in $N_s \to \infty$ could also be seen in the scaling relations (66)–(68). The coefficients C_1 and C_2 represent the magnitudes of the explicit breaking of chiral symmetry. C_1 is the additive mass counterterm, while C_2 is the mismatch between the quadratic terms of scalar and pseudoscalar particles by a quantum correction. If we restrict the DW mass to $0<M<2$, as shown in Fig. 2, the coefficients C_1 and C_2 decrease rapidly as N_s becomes large. The effects of shifting of the fields and the additive renormalization of the mass parameter in Eqs. (65) and (68) rapidly vanish with increasing N_s; thus the necessity of fine-tuning becomes absent in the $N_s \to \infty$ limit.

On the other hand, even when M is set out of the region (0,2), the scaling relations (66)–(68) lead the chiral symmetric continuum limit. In this case C_1 and C_2 do not vanish in the large N_s limit and fine-tuning is necessary, similar to the WF.

IV. PARITY BROKEN PHASE AND THE RESTORATION OF CHIRAL SYMMETRY

For lattice QCD with the WF, the existence of a massless pion for finite lattice spacing is explained by the parity broken phase picture proposed by Aoki [16]. Although chiral symmetry is explicitly broken in the WF, one can tune the mass parameter to obtain an exact *massless* pion in the spectrum even for finite lattice spacing. This cannot be understood by the ordinary picture of Nambu-Goldstone bosons in continuum theory, in which chiral symmetry is the exact symmetry of the action and is broken spontaneously.

Aoki examined the GN model and lattice QCD with the WF for a finite lattice spacing, and found that the parity symmetric phase and parity (flavor) spontaneously broken phase coexist in the parameter space of the model. The parity broken phase is characterized by the nonzero condensation of the pseudoscalar density, $\langle \Pi \rangle = \langle \psi i \gamma_5 \psi \rangle \neq 0$. Provided a second-order phase transition separating the two phases from each other, the pion becomes massless at the phase transition point, which is regarded as a massless particle accompanying the continuous phase transition.

Before starting an analysis of the phase diagram of the DWF model for general N_s, we note the equivalence between the $N_s=1$ DWF model and the Wilson fermion formalism. The effective potential of the WF,

$$V_{\mathrm{W}} = \frac{1}{2g_\sigma^2}(\sigma - m_f)^2 + \frac{1}{2g_\pi^2}\Pi^2 - \int_{-\pi/a}^{\pi/a} \frac{d^2k}{(2\pi)^2} \ln\left[\sum_\mu \frac{\sin^2 k_\mu a}{a^2} + \left(\sigma_c + \frac{r}{a}\sum_\mu (1-\cos k_\mu a) \right)^2 + \Pi_c^2 \right], \quad (69)$$

can be seen easily by substituting $N_s=1, \sigma_c = \sigma - (1-M)$ in Eq. (35). The phase boundary of Aoki phase forms three cusps which reach the weak-coupling limit $g^2=0$ at $M=1,3,5$ in the WF [16–18] and $N_s=1$ DWF models. Three cusps arise from the fact that the doublers at the conventional continuum limit, $(g^2,M)=(0,1)$, become physical massless modes at $M=3,5$.

On the other hand, in the $N_s=\infty$ limit, the parity broken phase does not exist because of the restoration of chiral symmetry, whose explicit breaking causes the parity broken phase.

For $1<N_s<\infty$, it is expected that the parity broken phase exists and the chiral phase boundary forms the cusps as surmised from the Wilson-like behavior in the previous section. The region of the broken phase is distorted and shrinks rapidly as N_s is increased, and vanishes in $N_s \to \infty$ limit.

The parity symmetry is spontaneously broken at the parameter point (m_f, g^2, M, N_s), where the gap equations have a stable solution $\Pi \neq 0$. Setting the parameters of this model $(m_f, g_\sigma^2, g_\pi^2, M, N_s)$, observables are calculated by solving the gap equations

$$\frac{\partial V_{eff}}{\partial \sigma} = \frac{1}{g_\sigma^2}(\sigma - m_f) - \sigma \mathcal{F}(\sigma,\Pi) - \frac{1}{a}\mathcal{G}(\sigma,\Pi) = 0, \quad (70)$$

$$\frac{\partial V_{eff}}{\partial \Pi} = \Pi \left[\frac{1}{g_\pi^2} - \mathcal{F}(\sigma,\Pi) \right] = 0, \quad (71)$$

where

$$\mathcal{F}(\sigma,\Pi) = \int_{-\pi}^{\pi} \frac{d^2\xi}{(2\pi)^2} \frac{2F}{H + Ga\sigma + Fa^2(\sigma^2+\Pi^2)}, \quad (72)$$

$$\mathcal{G}(\sigma,\Pi) = \int_{-\pi}^{\pi} \frac{d^2\xi}{(2\pi)^2} \frac{G}{H + Ga\sigma + Fa^2(\sigma^2+\Pi^2)}, \quad (73)$$

with $\xi_\mu = p_\mu a$. In the case of $g_\pi^2 = g_\sigma^2 = g^2$, the position of the phase boundary in parameter space could be obtained by solving these gap equations for $\Pi = \epsilon$. Taking the $\epsilon \to 0$ limit, Eqs. (70),(71) define g^2 and m_f as functions of σ which is nothing but the parametric representation of the phase boundary if the phase transition is continuous.

Let us note that the DWGN model with $g^2 = g_\sigma^2 = g_\pi^2$ has only a second-order phase transition between the parity symmetric and the broken phases. For $g_\sigma^2 \neq g_\pi^2$, see Ref. [22] in the WF case, in which a first-order phase transition is found.

By differentiating Eq. (71) with respect to Π, one can easily check that the pion mass squared

$$M_\pi^2 \propto \tilde{M}_\pi^2 \equiv \frac{1}{f_M^2}\frac{\partial^2 V_{eff}(\sigma,\Pi=0)}{\partial \Pi^2} = \frac{1}{f_M^2}\left[\frac{1}{g^2} - \mathcal{F}(\sigma,\Pi=0) \right] \quad (74)$$

exactly vanishes at the phase boundary. The factor, $1/f_M^2$, in front of the RHS corrects the normalization of the auxiliary field Π in the same sense as explained in the previous section. (See below Eq. (41).)

Before drawing whole phase diagrams in the parameter space (m_f, g^2), let us first examine the positions of the three

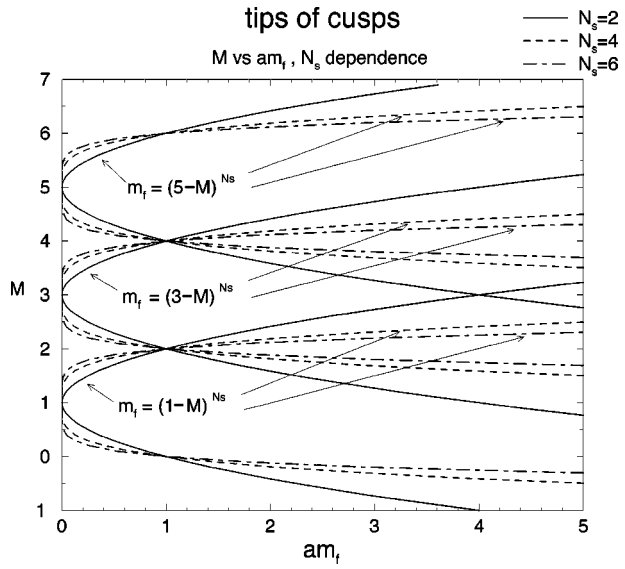

FIG. 3. The chiral symmetric continuum limit in the (M,am_f) plane for N_s=even. The critical lines approaches $m_f=0$ with increasing N_s in each of three regions, $2l<M<2(l+1)$, $l=0,1,2$.

''tips of cusps,'' which are the intersection points between $g^2=0$ plane and the critical line. These tips correspond to the continuum limits $g^2\to 0$ similar to the WF. The positions can be obtained by the asymptotic form of the integrals in Eqs. (70) and (71). The divergent behaviors of the integrals around $p_\mu a=(\pi m,\pi n)$, with $m,n=0$ or 1, are

$$\mathcal{F}(\sigma,\Pi=0)\to \sum_{m,n=0,1,l=m+n}\int_{-\pi}^{\pi}\frac{d^2\xi}{(2\pi)^2} \times\frac{2}{\{\sigma-(1-M+2l)^{N_s}\}^2+\sum_\mu \mathcal{A}_\mu\xi_\mu^2}, \qquad (75)$$

$$\mathcal{G}(\sigma,\Pi=0)\to \sum_{m,n=0,1,l=m+n}\int_{-\pi}^{\pi}\frac{d^2\xi}{(2\pi)^2} \times\frac{-2(1-M+2l)^{N_s}}{\{\sigma-(1-M+2l)^{N_s}\}^2+\sum_\mu \mathcal{B}_\mu\xi_\mu^2}, \qquad (76)$$

where $\mathcal{A}_\mu$ and $\mathcal{B}_\mu$ are functions of l, σ, M, and N_s. From these expressions it is easy to see that the RHS of the gap equations (70),(71) have a logarithmic divergence at $\sigma=(1-M+2l)^{N_s}$ with $l=0,1,2$. This fact leads to, for each l, the phase boundary intercepting with $g^2=0$ at a point $m_f=(1-M+2l)^{N_s}$. Each of three critical points corresponds to the massless particle pole of momentum

$$p_\mu(l=0)=(0,0),\quad p_\mu(l=1)=(\pi/a,0),(0,\pi/a),$$
$$p_\mu(l=2)=(\pi/a,\pi/a). \qquad (77)$$

The positions of three points move as a function of M, which is shown in Fig. 3. For M in the region of $(2l,2(l+1))$, the chiral point for the momentum mode $p_\mu(l)$ in Eq. (77) converges to $m_f=0$ as N_s increases. Thus a massless pion can be automatically obtained at $m_f=0$ in the limit of $g^2=0$ by increasing N_s. Other two critical points move rapidly to $|m_f|\to\infty$ in $N_s\to\infty$ limit.

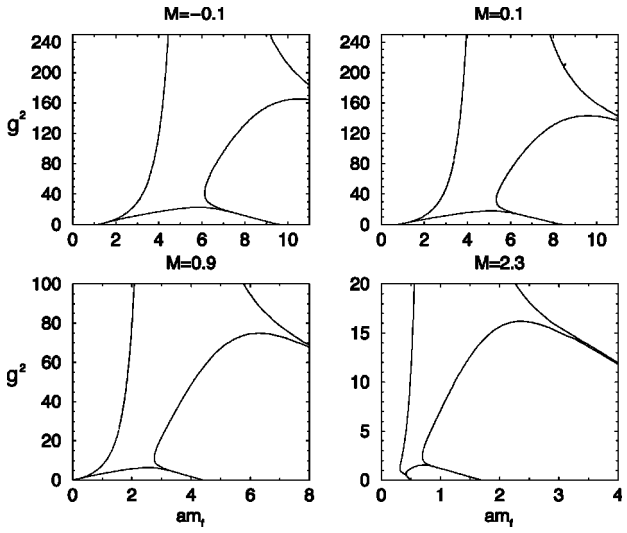

FIG. 4. The phase diagram at $N_s=2$. The horizontal axis represents am_f while the vertical axis is g^2. Each of four graphs is plotted for fixed value of M. The inside region of the critical line is the parity broken phase.

The actual calculation for the chiral phase boundary is done by solving the gap equations numerically, and results are shown in Figs. 4, 5, 6, and 7. The former two figures are for N_s=even cases and the latter two show N_s=odd cases.

The schematic diagram of the phase boundary between the parity symmetric and broken phase in (m_f,g^2) plane for fixed (M,N_s) is drawn in Fig. 8 for the N_s=even case and in Fig. 9 for N_s=odd. The phase boundaries in both cases show queer shapes which have three intercept points, $m_f=(1-M+2l)^{N_s}$ with $l=0,1,2$, on the $g^2=0$ line.

We find that the phase diagram for N_s=even is different from that for N_s=odd. In the N_s=even case, one can ana-

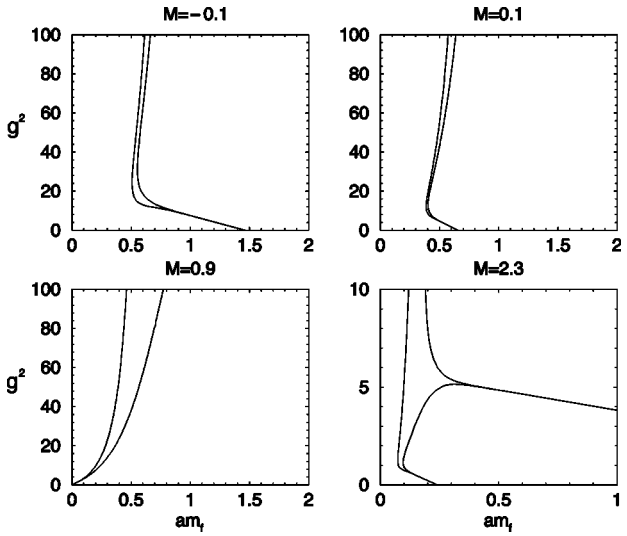

FIG. 5. The phase diagrams at $N_s=4$.

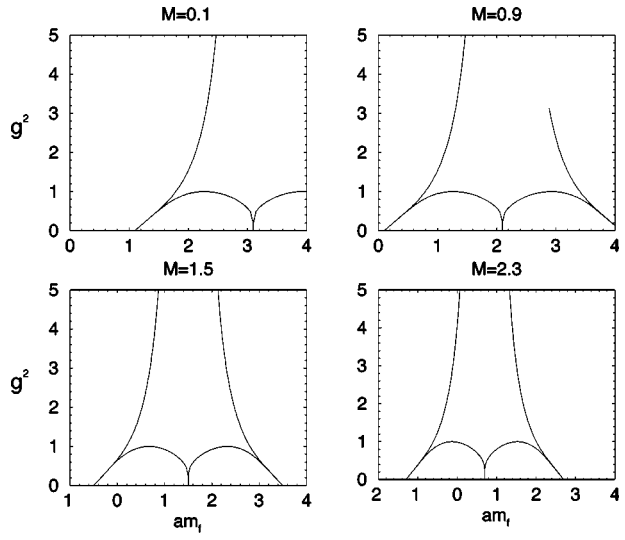

FIG. 6. The phase diagrams at $N_s=1$.

lytically verify from the sign definiteness of integrands of the gap equations that the phase boundary exists only for the $m_f>0$ region. (For the notation in Ref. [23] and numerical simulations, the broken phase always appears in the $m_f<0$ region.) On the other hand, the phase boundary intersects with the $m_f=0$ line in the $N_s=$odd case. If g^2 is decreased from a finite value to zero, the phase boundary moves from the positive m_f region to $m_f=(1-M+2I)^{N_s}$ at $g^2=0$, which becomes negative in some region of M for $N_s=$odd. The chiral phase boundaries for $N_s=$odd are shown in Figs. 6 and 7. The parity broken phase lies across the $m_f=0$ plane in the $N_s=$odd case. Similarly for $N_s=$even, this boundary for odd N_s also converges to the $m_f=0$ plane for larger N_s.

Another interesting observation from the phase diagram is the finite g^2 effect for the pion mass. The effective quark mass from the free propagator analysis (mean field analysis) is

$$m_q a \sim (M_c - M)^{N_s}, \tag{78}$$

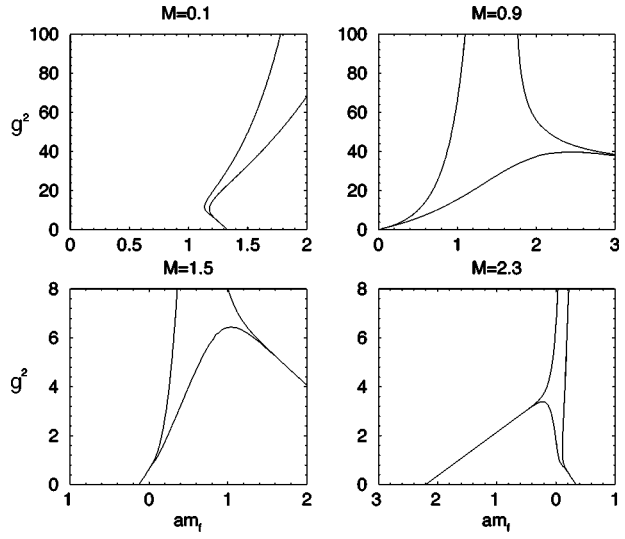

FIG. 7. The phase diagrams at $N_s=3$.

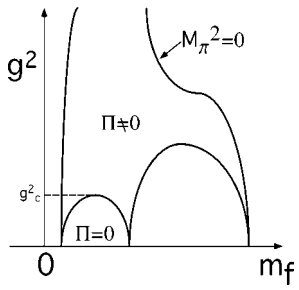

FIG. 8. The schematic phase diagram in the (m_f, g^2) plane for $N_s=$even. The parity broken phase exists in the $m_f>0$ region.

from which one may think that there exists optimal $M(=M_c)$, where the quark (and pion) becomes massless even for finite N_s. In the current model, for finite N_s the parity broken phase boundary stays apart from the $m_f=0$ plane *for all* M if $g^2>0$. This fact indicates that there is no massless pion at $m_f=0$ for finite N_s and finite g^2. We plot the value of m_f where $M_\pi^2=0$ as a function of M in Fig. 10. (This is the distance of the phase boundary point from the $m_f=0$ line. This quantity corresponds to the critical value of the inverse hopping parameter, $1/\kappa_c$, in the WF.) We find that for fixed finite N_s and finite g^2, the pion does not become massless at $m_f=0$. We realize that this discrepancy from the mean field picture in Eq. (78) is due to the part of the additive mass term which is proportional to C_1 in Eq. (68). For strong coupling, for example, $g^2=5.0$, $m_f(M_\pi=0)$ is almost flat at around $M\sim 2.0$. This indicates a difficulty of detecting the ''allowed region'' of M by observing the pion mass for the strong coupling region. For $g^2=0$ the theory turns out to be a free theory, and $M=1$ gives $M_\pi=0$ at $m_f=0$. If N_s is increased, $m_f(M_\pi=0)$ becomes an exponentially small convergence to zero no matter whether g^2 is finite or 0. (See Fig. 11.)

The dependence of the phase diagram on N_s can be seen in Fig. 12. In the figure for $M=0.9$, the cusp of smaller m_f corresponds to the chiral continuum limit of the conventional momentum mode $p_\mu=(0,0)$ and other cusps show that of the doubler modes. The first cusp converges to the $m_f=0$ line while the other cusps diverge to $m_f\to\infty$ in the large N_s limit. Below a critical coupling, g_c^2, in Figs. 8 and 9, a pair of critical lines forms either of three continuum limits (three cusps) similar to the WF, which can be understood as the signal for the recovery of chiral symmetry. For $g^2>g_c^2$ the

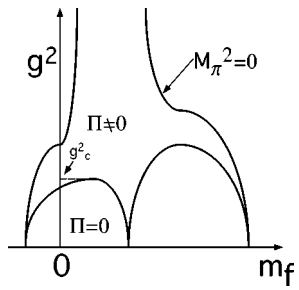

FIG. 9. Same as Fig. 8 for $N_s=$odd. The parity broken phase lies across the $m_f=0$ line.

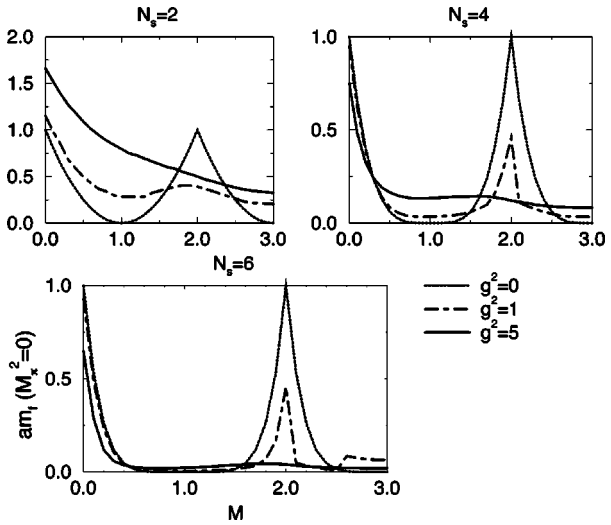

FIG. 10. The distance from the $m_f=0$ line to the phase boundary, $m_f(M_\pi=0)$, which corresponds to the critical value of the current quark mass, as a function of M for fixed N_s, g^2.

parity broken phases are merged to a uniform structure. We find that g_c^2 increases exponentially with N_s:

$$g_c^2 \sim e^{cN_s} \quad (c>0). \tag{79}$$

At the same time, the phase boundary exponentially approaches the $m_f=0$ plane with increasing N_s. For any g^2, the phase boundaries converge at the $m_f=0$ plane, which can be easily seen from Eqs. (70) and (71). The width of the parity broken phase scales proportional to a^3 [25], and shrinks exponentially for $N_s\to\infty$. These facts are compatible with the exact chiral symmetry for finite lattice spacing in the $N_s\to\infty$ limit, as discussed in the previous section.

On the other hand, at $M=-0.1$ the chiral continuum limit and the phase boundary go away from the $m_f=0$ line with

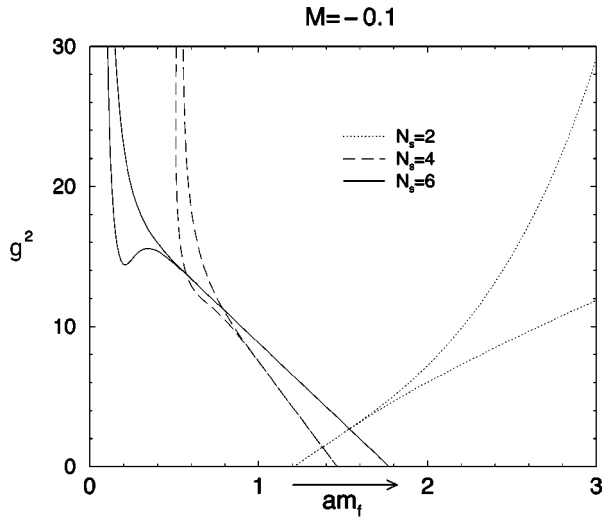

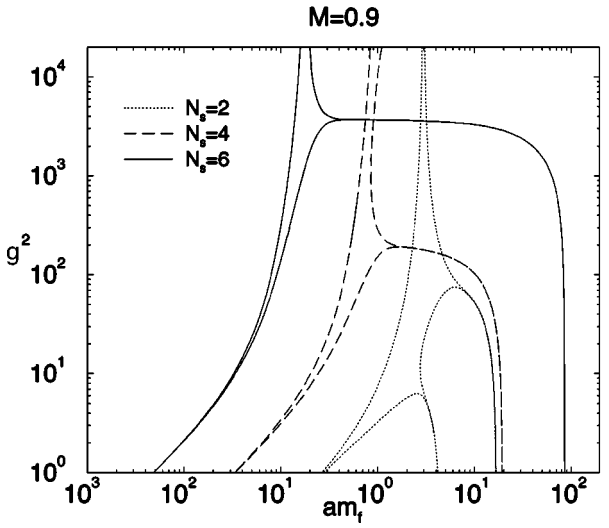

FIG. 12. N_s dependence of the phase boundary for $M=-0.1, 0.9$. The horizontal axis represents m_f while the vertical axis is g^2.

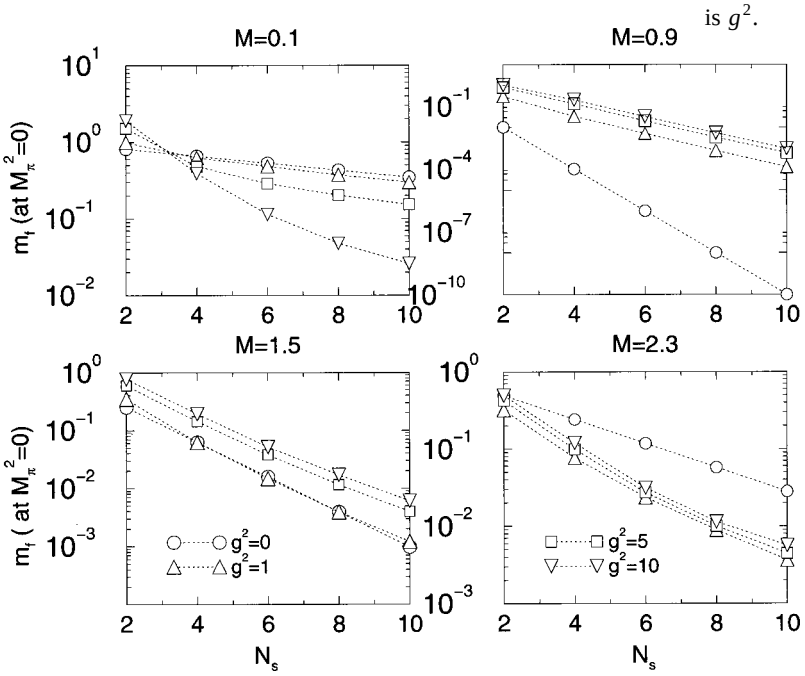

FIG. 11. $m_f(M_\pi=0)$ as a function of N_s for fixed M, g^2.

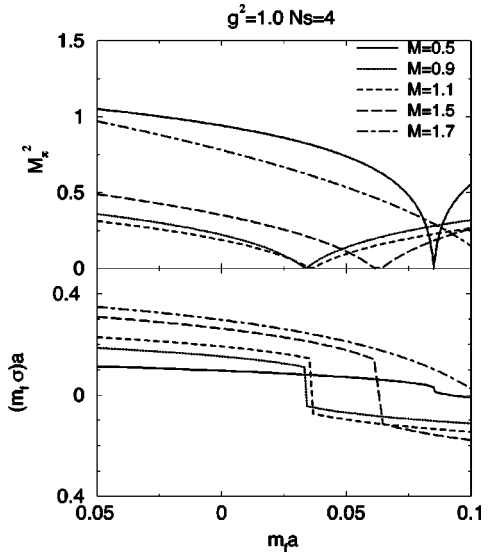

FIG. 13. $\tilde{M}_\pi^2$ and $\langle\bar{q}q\rangle = m_f - \sigma$ as a function of m_f. $N_s = 4$, $g^2 = 1.0$.

increasing N_s. This behavior shows the violation of chiral symmetry at $m_f = 0$ even in the $N_s \to \infty$ limit for $M < 0$.

V. (M,N_s) DEPENDENCES OF LATTICE OBSERVABLES

Let us turn to discuss the physical observables in this model. We choose σ, $\langle\bar{q}q\rangle$, and $\tilde{M}_\pi$ as the physical observables.

In Fig. 13 we plot $\tilde{M}_\pi^2$ and $\langle\bar{q}q\rangle \equiv m_f - \sigma$ as a function of m_f for several values of M with $g^2 = 1, N_s = 4$. We find that there exists a finite m_f region in which M_π is zero.[2] This region is nothing but the parity broken phase. The m_f dependence of the $\langle\bar{q}q\rangle$ shows a discontinuous leap in between the parity broken phase.

The systematic dependences of observables on the parameter M are shown in Figs. 14 and 15. In Fig. 14 we plot $\langle\bar{q}q\rangle$ as a function of M for several m_f with $g^2 = 1$ and $N_s = 20$. $\langle\bar{q}q\rangle$ continuously gains in magnitude with increasing M around $M \sim 1$. $\langle\bar{q}q\rangle$ for $m_f = 0$ turns out to have a minimum magnitude around $M \sim 2$.

$\tilde{M}_\pi^2$ also has a systematic dependence on M. Because the ratio $\tilde{M}_\pi^2 / M_\pi^2$ is a smooth function of M and N_s, $\tilde{M}_\pi^2$ shows essential characteristics of the pion mass. In Fig. 15, $\tilde{M}_\pi^2 f_M^2 = d^2 V_{eff} / d\Pi^2$ is plotted against M. Comparing the results of strong coupling ($g^2 = 5.0$) with that of weak coupling ($g^2 = 1.0$) in this figure, we find that the depression of $\tilde{M}_\pi^2 f_M^2$ near $M \sim 1$ for weak coupling is not very manifest for strong coupling especially in the small N_s limit. In fact the minimum of $\tilde{M}_\pi^2 f_M^2$ places at $M > 2$ for $N_s = 4$. This implies that in order to find the allowed region of M for the chiral continuum limit by observing the depression of the pion mass, one needs larger N_s for strong coupling than that needed for weak coupling in DWQCD simulations. Note that such an allowed region of M is unknown *a priori* in QCD by the additive quantum corrections.

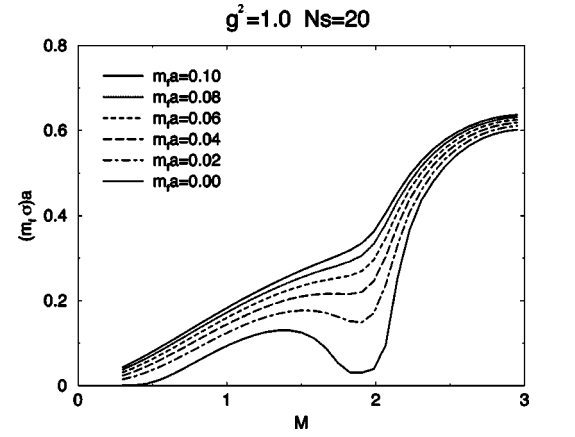

FIG. 14. $\langle\bar{q}q\rangle = m_f - \sigma$ as a function of M. $N_s = 20$, $g^2 = 1.0$.

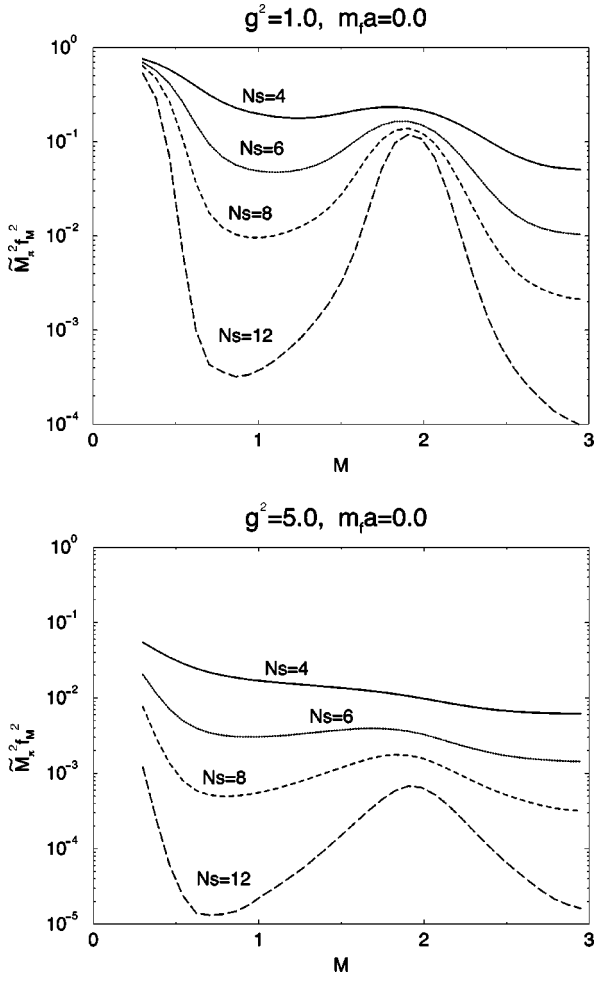

FIG. 15. $\tilde{M}_\pi^2 f_M^2$ as a function of M. $g^2 = 1.0$ and $g^2 = 5.0$ for $N_s = 2,4,6,8,12$.

[2]We set $\Pi = 0$ throughout our calculation, and the value of physical observables in the parity broken phase is not exact. For example, M_π^2 should not be zero in the parity broken phase. Note that all figures after this section except Fig. 13 are obtained in parity symmetric parameter region, in which our results are precise.

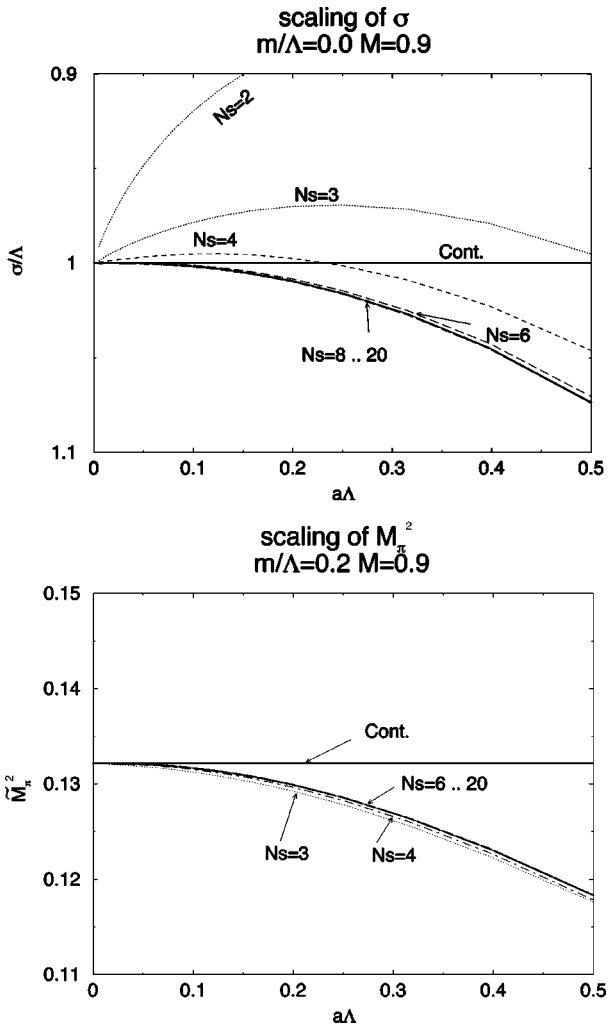

FIG. 16. σ/Λ and $\tilde{M}_\pi^2$ as a function of $a\Lambda$ for fixed M. The continuum limit is taken using the (Wilson like) scaling relations in Eqs. (66)–(68).

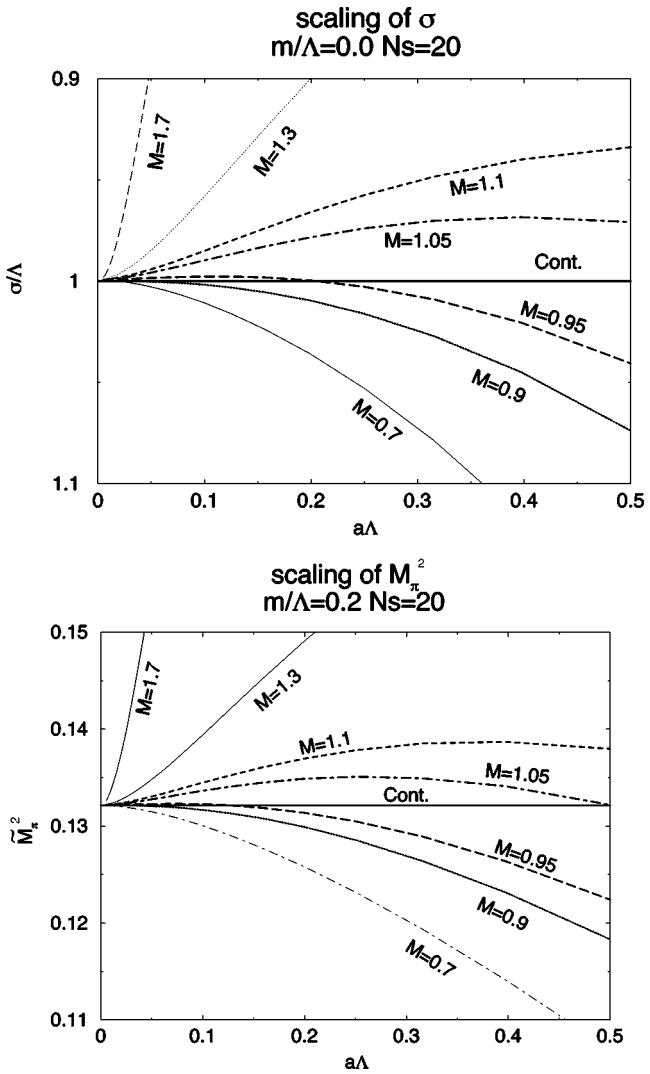

FIG. 17. σ/Λ and $\tilde{M}_\pi^2$ as a function of $a\Lambda$ at $Ns=20$.

As we pointed out in the previous section, the pion mass does not vanish for all M at $m_f=0$ for finite N_s if $g^2>0$. For $N_s=4$, $\tilde{M}_\pi^2$ at $m_f=0$ has its minimum at around $M=1.4$. For larger N_s, $\tilde{M}_\pi^2(m_f=0)$ in the region $0<M<2$ tends to be flat with smaller pion mass. From this figure we conclude that chiral symmetry is restored for large N_s if M is set in the region $0<M<2$. There is another region $2<M<4$, where the pion would be a massless particle in the $N_s\to\infty$ limit. This region corresponds to the region of massless ''pion,'' which is made of the chiral modes at $p_\mu a=(\pi,0),(0,\pi)$.

VI. CONTINUUM LIMIT AND DISAPPEARANCE OF $O(a)$ SCALING VIOLATIONS

Toward the continuum limit $a\to 0$, the lattice bare parameters are tuned according to the scaling relation (66)–(68) for finite N_s. We plot σ and M_π^2 as a function of the lattice spacing $a\Lambda$ in Fig. 16 for several N_s with fixed DW mass $M\sim 1$.

The lattice bare observables systematically depend on M as shown in the previous section. From Eq. (67) the lattice spacing (or the scale parameter of the theory) is also a function of M,

$$\Lambda a(M,N_s)=\exp\left[-\frac{2\pi}{f_M^2}\left(\frac{1}{2g_\pi^2}-\hat{C}_0(M,N_s)\right)\right]. \quad (80)$$

See Fig. 1 for the (M,N_s) dependence of $\hat{C}_0$. The M dependences of observables cancel with that of the lattice spacing, and the correct continuum values are reproduced at the $a\to 0$ limit. (See Fig. 16.)

An interesting observation is the disappearance of the $O(a)$ scaling violation for the large N_s limit. From the theoretical point of view, exact chiral symmetry in $N_s\to\infty$ limit is expected to prohibit the dimension $(D+1)$ operators in the quantum correction, which cause an $O(a)$ scaling violation. The slope at the $a\Lambda=0$ curve in Fig. 16 is finite at $N_s=2$ while the curve at $N_s=20$ is flat near $a\Lambda=0$. This shows that the $O(a)$ scaling violation vanishes in the large N_s limit and a scaling violation proportional to a^2 exists.

Figure 17 shows that the remaining $O(a^2)$ error is small

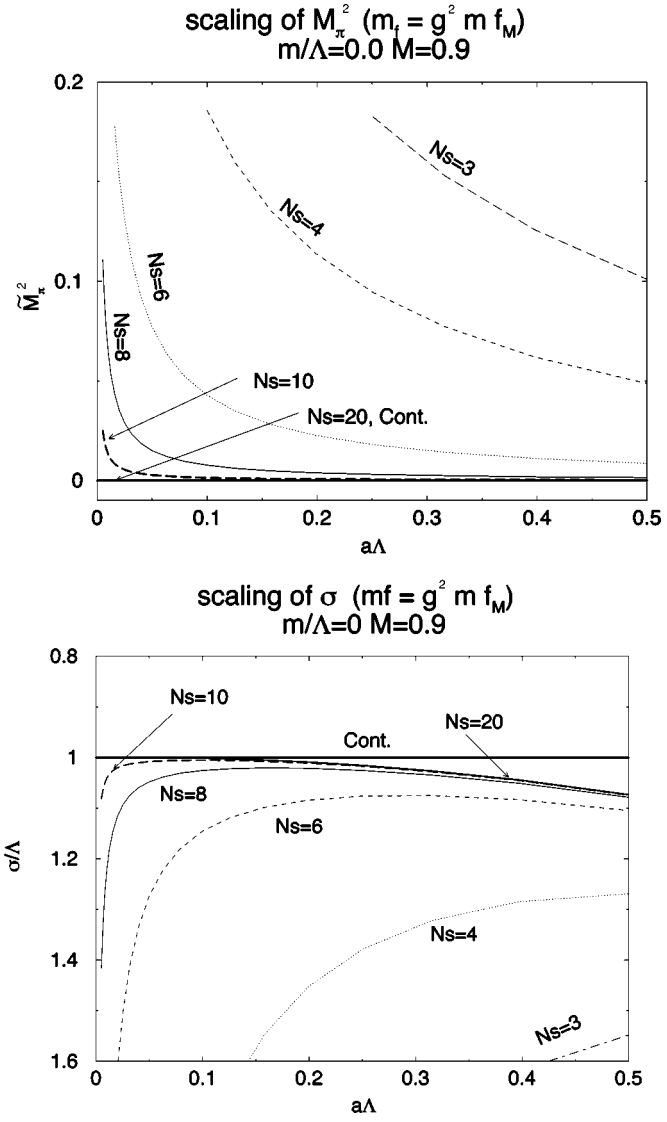

FIG. 18. σ/Λ and $\tilde{M}_\pi^2$ as a function of $a\Lambda$ at $M=0.9$. The DWF scaling relations in Eqs. (82)–(84) are employed.

for $M\sim 1$ in the large N_s limit, which is less than a few percentage for $a\Lambda<0.5$ in this model. The reason why this $O(a^2)$ scaling violation is small near $M=1$ could be understood by expanding the inverse integrand of the function ''$I_0(\sigma,\Pi)$'' for small a:

$$\frac{H'}{Fa^2}=p^2/f_M^2+cp^4/f_M^4a^2+c'p^6/f_M^6a^4+\cdots. \tag{81}$$

Since $1/f_M$ is minimum at $M=1$, the $O(a^2)$ deviation from the continuum formula is also minimum for $M=1$. This feature might be similar for QCD simulations, except M receives additive renormalization from the quantum fluctuation of the gauge field.

The renormalization formula employed above for finite N_s is similar to that of the WF. The bare mass needs to be

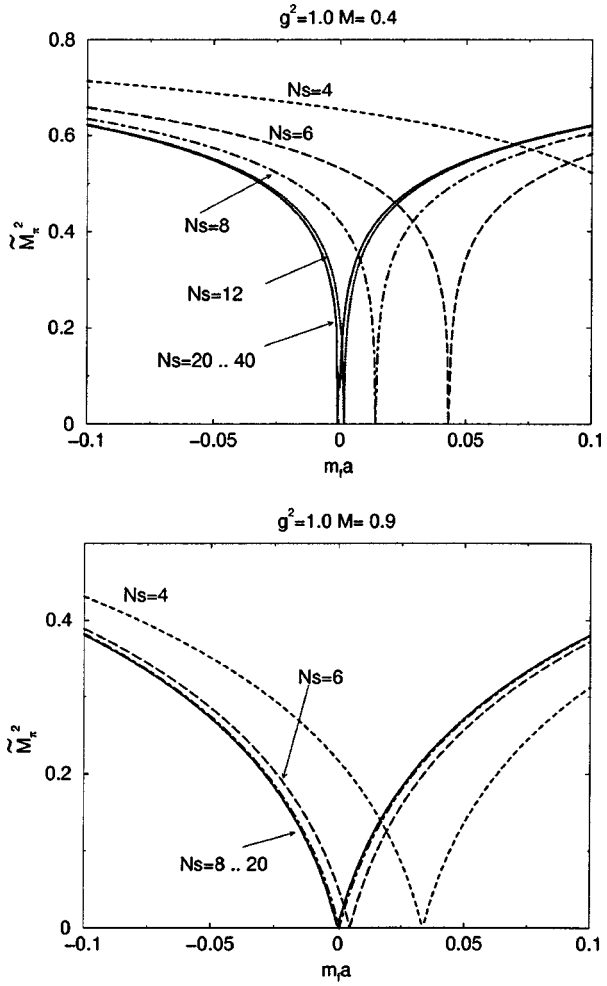

FIG. 19. N_s dependence of $\tilde{M}_\pi^2$ as a function of m_f.

fine-tuned toward a certain critical value. On the other hand, we consider applying the scaling relation for $N_s\to\infty$ (without fine-tuning),

$$\frac{1}{2g_\sigma^2}-\hat{C}_0+C_2=\frac{f_M^2}{4\pi}\ln\frac{1}{a^2\Lambda^2}, \tag{82}$$

$$g_\pi^2=g_\sigma^2, \tag{83}$$

$$\frac{1}{f_M}\frac{m_f}{g_\sigma^2}=m, \tag{84}$$

to *finite* N_s lattice observables. This is similar to what is done in the DWQCD simulation in a sense. The result of this calculation for finite N_s is shown in Fig. 18. For each N_s, $\tilde{M}_\pi^2$ is apt to go to the correct continuum value for large $a\Lambda$ but tends to diverge for smaller lattice spacing. Such divergent behavior is never seen in current DWQCD simulations [14,15] since $a\Lambda_{\rm QCD}$ is larger than 0.1.

From Eq. (68) the renormalized mass is expressed as a function of the bare quark mass m_f:

$$ma = \frac{1}{f_M g^2}[m_f a - (1-M)^{N_s} + g^2 C_1(M,N_s)]. \quad (85)$$

For each g^2 (and $a\Lambda$), if N_s fulfills a condition

$$N_s > N_s^c \text{ s.t. } |am_f| \gg |-(1-M)^{N_s^c} + g^2 C_1(M,N_s^c)|, \quad (86)$$

the renormalized mass approximately becomes that in the $N_s \to \infty$ case. Such N_s^c can exist for finite m_f if $0<M<2$ because both $(1-M)^{N_s}$ and $C_1(M,N_s)$ go to zero for large N_s. Thus, if N_s is larger than N_s^c, physical predictions from DWF are saturated as a function of N_s and could be regarded as the value of $N_s \to \infty$. N_s^c is a function of g^2, M, and m_f, and tends to be larger for smaller m_f. The N_s dependence of $\tilde{M}_\pi^2$ could be seen in Fig. 19. For a large magnitude of m_f the N_s dependence is saturated up to $N_s \sim 12$, while $\tilde{M}_\pi^2$ varies as a function of N_s near $m_f=0$. From this figure for $(g^2,M)=(1,0.4)$, we can estimate that N_s^c is near 10 for $|m_f| \sim 0.1$ and $N_s^c \sim 20$ for $|m_f| \sim 0.02$. In this model N_s^c goes to a small value for $M \sim 1$. For $M=0.9$ the value of $\tilde{M}_\pi^2$ for $N_s=12$ is nearly identical to that of $N_s=20$ for almost all the region of m_f in Fig. 19.

VII. CONCLUSIONS AND DISCUSSIONS

We have investigated the two-dimensional lattice GN model with the DWF in the large flavor (N) limit, as the toy model of lattice QCD with the DWF. By calculating the effective potential we study the nonperturbative prospects of this model, which are expected to be qualitatively similar to DWQCD.

In the infinite N_s case, the effective potential has exact chiral symmetry even for finite lattice spacing. The chiral phase boundary is placed exactly on the $m_f=0$ line, which shows that the fine-tuning of the mass parameter m_f becomes needless. The parity broken phase does not exist for all coupling constants. Thus the model for $N_s=\infty$ has similar properties as the continuum theory especially for chiral symmetry, by which the massless pion could be understood as a NG boson accompanying the spontaneous breakdown of the symmetry.

The finite N_s case, for which numerical simulations are carried out, is practically important. Chiral symmetry is explicitly broken by the finite N_s effect, which causes a parity broken phase with $(D+1)$ cusps near $g^2=0$ similar to the Aoki phase of the WF. The restoration of chiral symmetry only occurs in the continuum limit with fine-tuning of m_f to its critical point, which is on the phase boundary of the parity broken phase. By increasing N_s for fixed a, the phase boundary exponentially approaches the $m_f=0$ plane in parameter space and the parity broken phase vanishes in $N_s \to \infty$. If one takes the limit $N_s \to \infty$ prior to the $a \to 0$ limit, chiral symmetry is restored.

Another interesting observation is the N_s dependence of the critical coupling g_c^2. For $g^2 < g_c^2$, the parity broken phase splits into $(D+1)$ regions, each of which corresponds to a chiral symmetric continuum limit. The restoration of the chiral symmetry is also characterized by the fact that g_c^2 exponentially goes to a large value with increasing N_s.

We also show (M,N_s) dependences of lattice bare observables, which could be some hints for DWQCD simulations. When N_s is finite and $g^2>0$, the pion mass at $m_f=0$ never goes to zero for all M. If M is set into the range (0,2), the pion mass at $m_f=0$ is exponentially suppressed with increasing N_s. From the results of m_f at $M_\pi=0$ (Fig. 10) and M_π at $m_f=0$ (Fig. 15), we discussed that one needs to take larger N_s for strong coupling than that needed for weak coupling in DWQCD simulations, in order to search the allowed region of M for the chiral continuum limit by observing the depression of the pion mass. By observing the N_s dependences of the observables we discuss the criterion $N_s > N_s^c$, for which the physical observables can be considered as approximate values for $N_s \to \infty$. N_s^c is a function of g^2, M, and m_f.

The observables depend on the value of M even for $N_s \to \infty$. This dependence is canceled by the renormalization and the correct continuum theory is obtained. The disappearance of the $O(a)$ scaling violation for large N_s in the continuum limit suggests the probability of obtaining reliable physical predictions for smaller lattice spacing than that in the WF.

Since the GN model in the large N limit neglects quantum fluctuations and omits gauge fields, we cannot insist that the behavior of lattice QCD with the DWF be exactly the same as the results in this paper. For example, the DW mass M is the shifted into $\tilde{M}=M+\text{const}$ due to the back reaction of the gauge fields. Another important difference between the GN model and DWQCD is the possibility of a zero mode along extra dimension. If the fluctuation of gauge fields in DWQCD makes part of the eigenvalues of the transfer matrix along the extra direction close to unity with a finite path-integral measure, the chiral symmetry of this model may be violated. To nail down such a disaster, eigenvalue problems for DWQCD are worth exploring. Work in this direction is in progress. Besides these different aspects, there are many similarities between the GN model and QCD, at least for the Wilson action [16–18]; we expect that the results shown in this paper will provide instructive and systematic information about the *nonperturbative* effects of lattice QCD with the DWF.

ACKNOWLEDGMENTS

We thank S. Aoki, Y. Kuramashi, Y. Taniguchi, and A. Ukawa for illuminating discussions and continuous encouragement. The numerical calculations for the present work have been carried out at the Center for Computational Physics at the University of Tsukuba. This work is supported in part by Grants-in-Aid for Scientific Research from the Ministry of Education, Science and Culture (Nos. 2375, 6769). The authors are supported by the Japan Society for Promotion of Science.

[1] H. B. Nielsen and M. Ninomiya, Nucl. Phys. **B185**, 20 (1981); **B195**, 541(E) (1982); **B193**, 173 (1981); Phys. Lett. **105B**, 219 (1981).
[2] L. H. Karsten, Phys. Lett. **104B**, 315 (1981).
[3] K. Wilson, in *New Phenomena in Subnuclear Physics*, edited by Zichichi (Plenum, New York, 1977).
[4] L. Karsten and J. Smit, Nucl. Phys. **B183**, 103 (1981).
[5] D. B. Kaplan, Phys. Lett. B **288**, 342 (1992); Nucl. Phys. B (Proc. Suppl.) **30**, 597 (1993).
[6] Y. Shamir, Nucl. Phys. **B406**, 90 (1993).
[7] S. Aoki and Y. Taniguchi, Phys. Rev. D **58**, 074505 (1998); Nucl. Phys. B (Proc. Suppl.) **63**, 20 (1998).
[8] Yoshio Kikukawa, Herbert Neuberger, and Atsushi Yamada, Nucl. Phys. **B526**, 572 (1998).
[9] Rajamani Narayanan and Herbert Neuberger, Nucl. Phys. **B412**, 574 (1994).
[10] Rajamani Narayanan and Herbert Neuberger, Nucl. Phys. **B443**, 305 (1995).
[11] H. Neuberger, Phys. Rev. D **57**, 5417 (1998).
[12] Rajamani Narayanan and Herbert Neuberger, Phys. Lett. B **302**, 62 (1993).
[13] V. Furman and Y. Shamir, Nucl. Phys. **B439**, 54 (1995).
[14] T. Blum and A. Soni, Phys. Rev. D **56**, 174 (1997); Phys. Rev. Lett. **79**, 3595 (1997); T. Blum, Nucl. Phys. B (Proc. Suppl.) **73**, 167 (1999).
[15] Columbia Lattice Group, P. Chen *et al.*, presented at the 29th International Conference on High-Energy Physics (ICHEP 98), Vancouver, Canada, 1998, in Vancouver 1998, High Energy Physics, Vol. 2*, pp. 1802–1808, hep-lat/9812011; P. Vranas and Columbia Lattice Group, contributed to American Physical Society (APS) Meeting of the Division of Particles and Fields (DPF 99), Los Angeles, CA, 1999, hep-lat/9903024.
[16] S. Aoki, Phys. Rev. D **30**, 2653 (1984).
[17] S. Aoki, A. Ukawa, and T. Umemura, Phys. Rev. Lett. **76**, 873 (1996).
[18] S. Aoki, T. Kaneda, and A. Ukawa, Phys. Rev. D **56**, 1808 (1997).
[19] Sinya Aoki and Kiyoshi Higashijima, Prog. Theor. Phys. **76**, 521 (1986).
[20] P. Vranas, I. Tziligakis, and J. Kogut, Phys. Rev. D (to be published), hep-lat/9905018.
[21] Ikuo Ichinose and Keiichi Nagao, Phys. Lett. B **460**, 164 (1999).
[22] T. Izubuchi, J. Noaki, and A. Ukawa, Phys. Rev. D **58**, 114507 (1998).
[23] P. Vranas, Phys. Rev. D **57**, 1415 (1998); Nucl. Phys. B (Proc. Suppl.) **63**, 605 (1998).
[24] Yoshio Kikukawa and Atsushi Yamada, Phys. Lett. B **448**, 265 (1999).
[25] Stephen Sharp and Robert Singleton, Jr., Phys. Rev. D **58**, 074501 (1998).